Supporting Information

Collapse or Capture? Guest-Induced Response of Two Structurally Distinct Pillared-MOFs upon exposure to Pyridines and Quinolines

Dario Giovanardi[a], Giorgio Cagossi[a], Pavel N. Zolotarev[b], Paolo P. Mazzeo[a], Alessia Bacchi[a], Lucia Carlucci[b], Davide M. Proserpio[b], Paolo Pelagatti[a,c]*

[a]Department of Chemical Science, Life Science and Environmental Sustainability, University of Parma, Parco Area delle Scienze 17/A, 43124 Parma, Italy.

[b]Dipartimento di Chimica, Università degli studi di Milano, 20133 Milano, Italy

[c]Interuniversity Consortium of Chemical Reactivity and Catalysis (CIRCC), Via Ulpiani 27, 70126 Bari, Italy

Index

Optical Microscopy Images

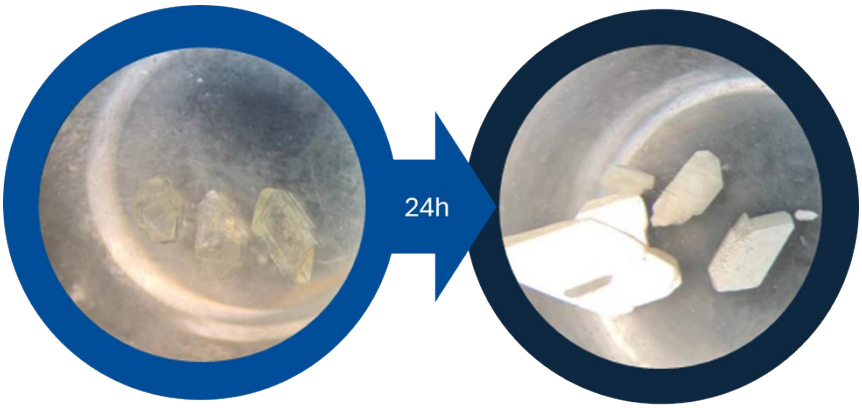

Figure S1 Photographs of the crystal of **PUM168** after soaking with 3-hydroxymethylpyridine.

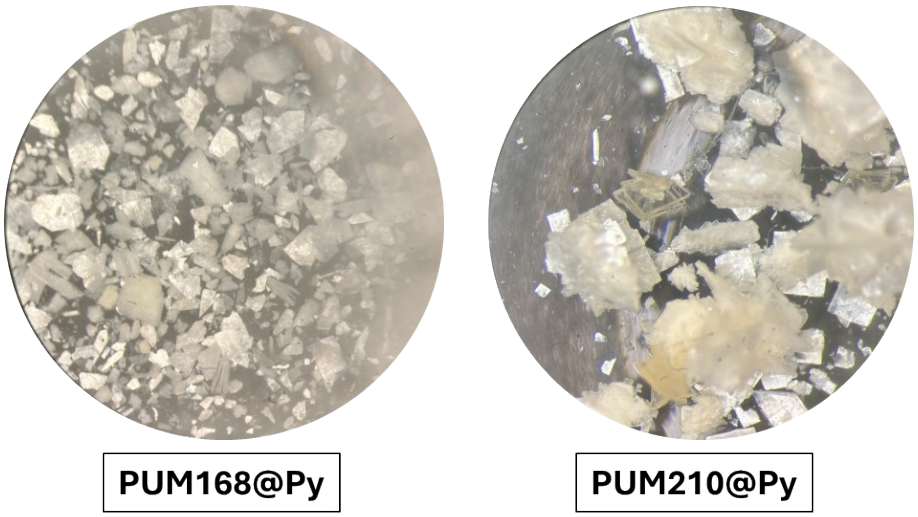

Figure S2. Comparison of the crystals of **PUM168** (left) and **PUM210** (right) after soaking in neat pyridine for 24 h. in both cases severe opacification and exfoliation of the crystals is evident. In case of **PUM210@Py** some block-shaped yellow crystals can be observed forming after 24 hours of soaking. These correspond to ligand **L1**, as evidenced by EDX analysis and SCXRD analysis.

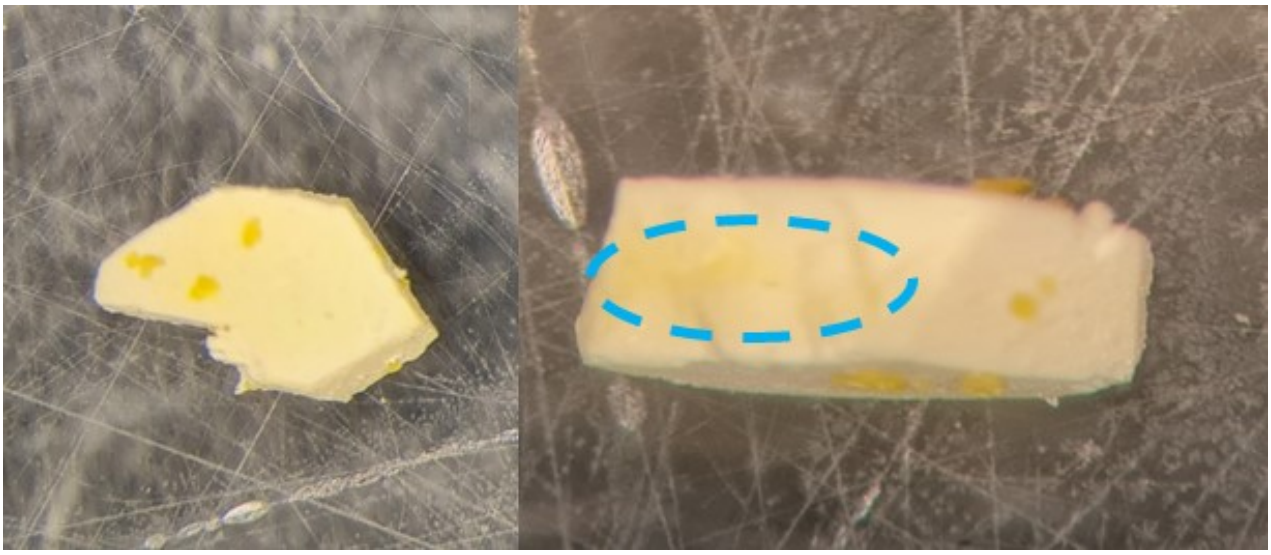

Figure S3. Comparison of the crystal of **PUM168** (left) after treatment with 8-hydroxy-quinoline showing the formation of yellow crystals of the **Zn(8-OH-quinolinate)$_2$** complex on the surface. On the right the same crystal after being cut to show the presence of a superficial effect determined by the slow diffusion of the guest in the material. The inner section of the crystal displays the retainment of **PUM168**, depicted from the yellow core.

^{1}H NMR

The quantification of the guest is done normalizing to 6 the area of the peak belonging to the protons in ortho position to pyridine nitrogen of **L1** (~9.1 ppm), based on the formula of the asymmetric unit of the starting MOF.

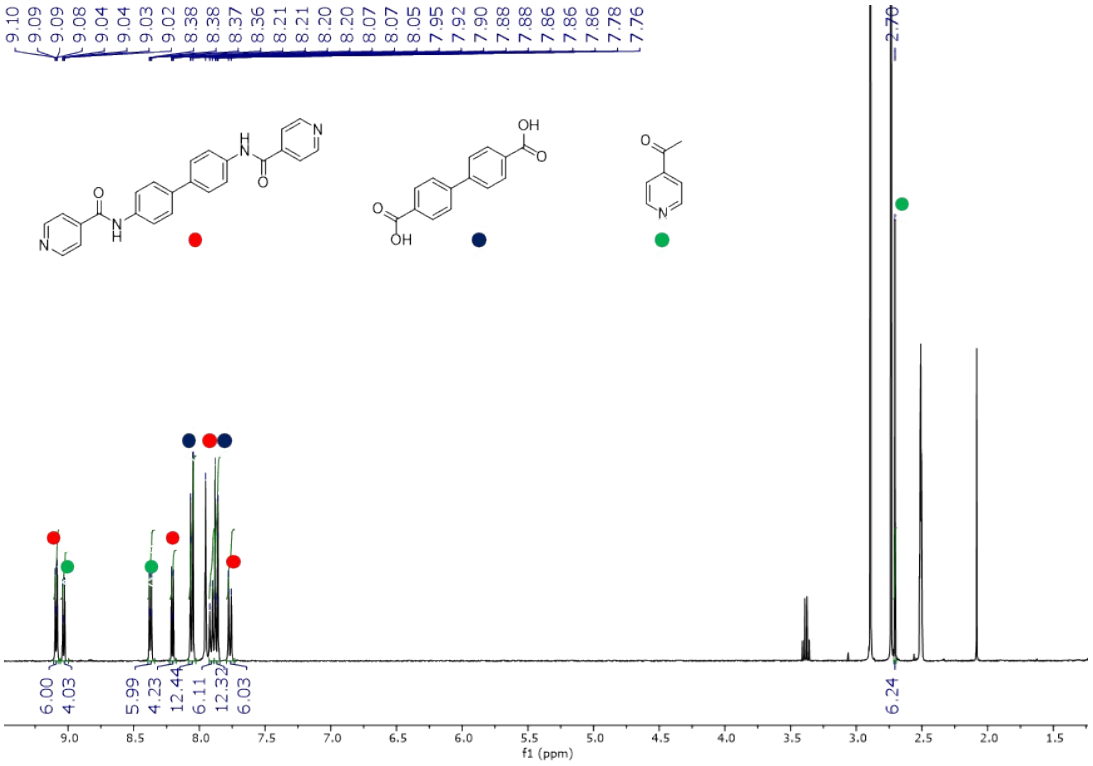

Figure S4. ^{1}H NMR spectrum of crystals of **PUM168@AcPyr** in DMSO-d_6 after digestion with one drop of TFA-d at 400 MHz, 25°C.

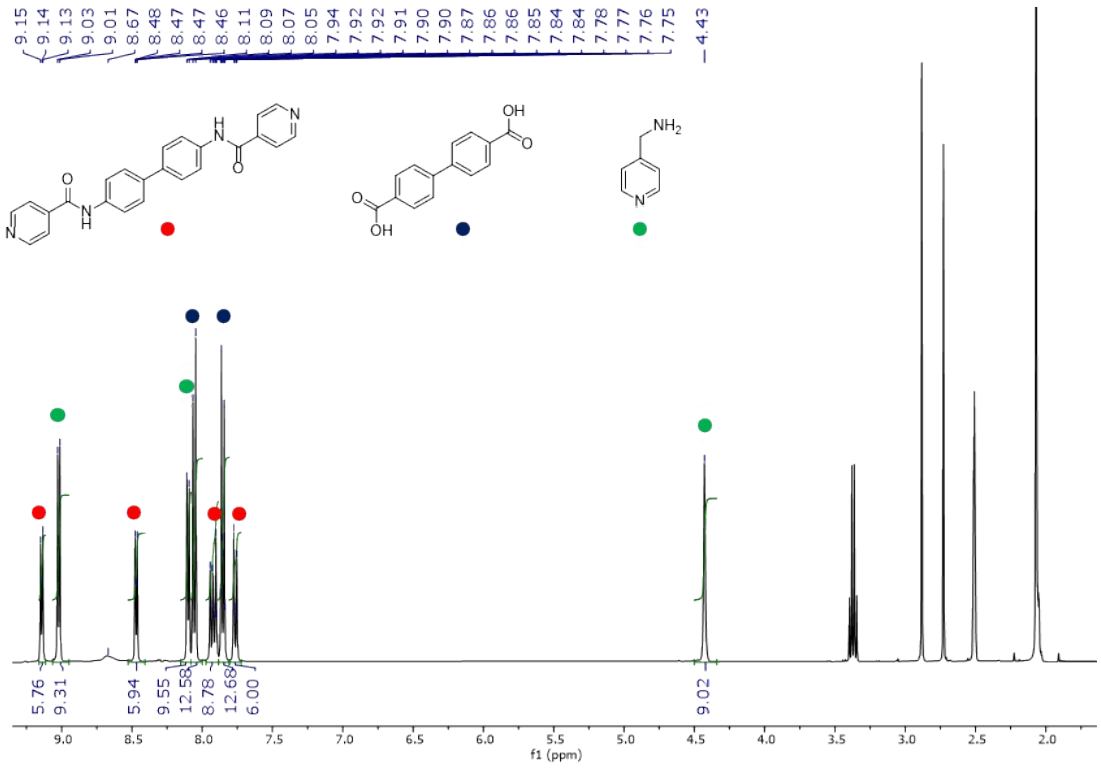

Figure S5. ^{1}H NMR of crystals of **PUM168@4NH$_2$MePyr** in DMSO-d$_6$ after digestion with one drop of TFA-d at 400 MHz, 25°C.

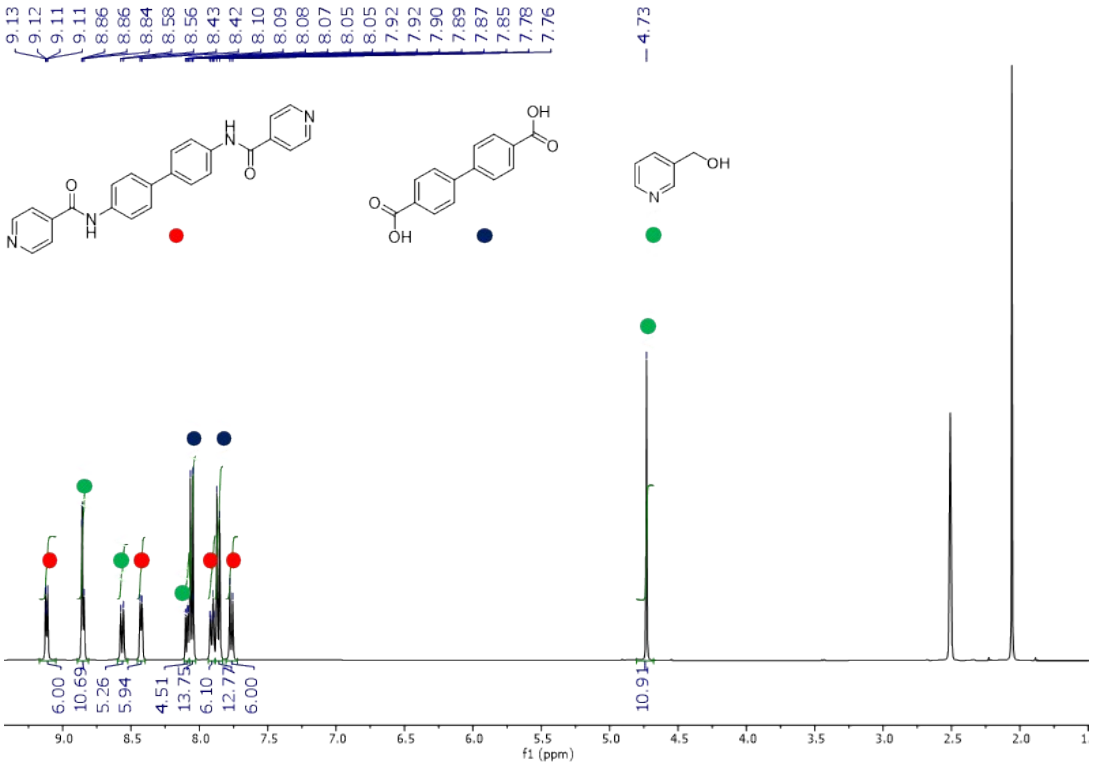

Figure S6. ^{1}H NMR of crystals of **PUM168@3OHMePyr** in DMSO-d$_6$ after digestion with one drop of TFA-d at 400 MHz, 25°C.

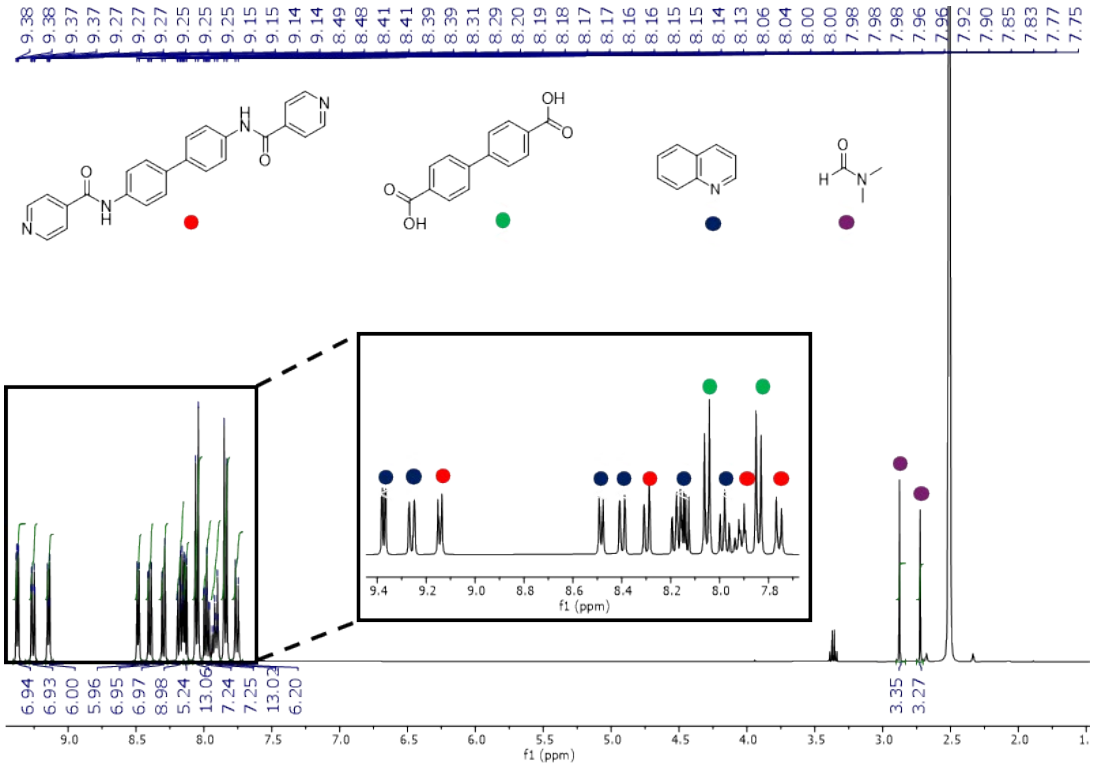

Figure S7. ^{1}H NMR of crystals of **PUM168@(quino)$_7$** in DMSO-d$_6$ after digestion with one drop of TFA-d at 400 MHz, 25°C.

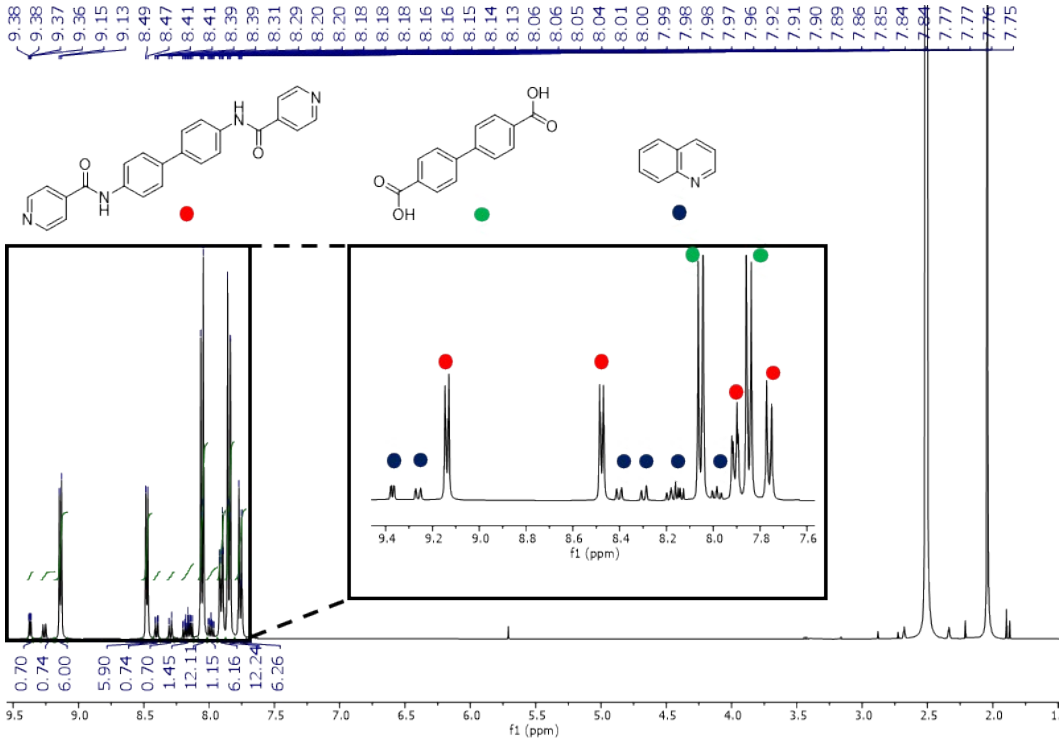

Figure S8. ^{1}H NMR of crystals of **PUM168@(quino)$_1$** in DMSO-d$_6$ after digestion with one drop of TFA-d at 400 MHz, 25°C.

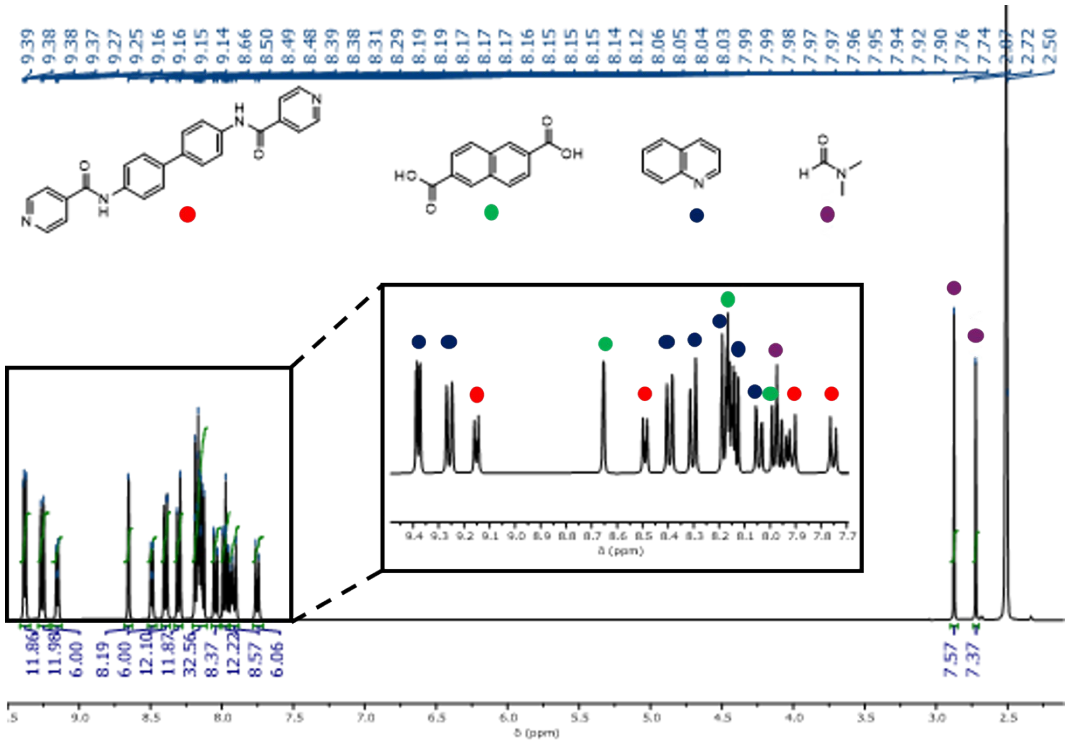

Figure S9. ^{1}H NMR of crystals of **PUM210@(quino)$_1$** in DMSO-d$_6$ after digestion with one drop of TFA-d at 400 MHz, 25°C.

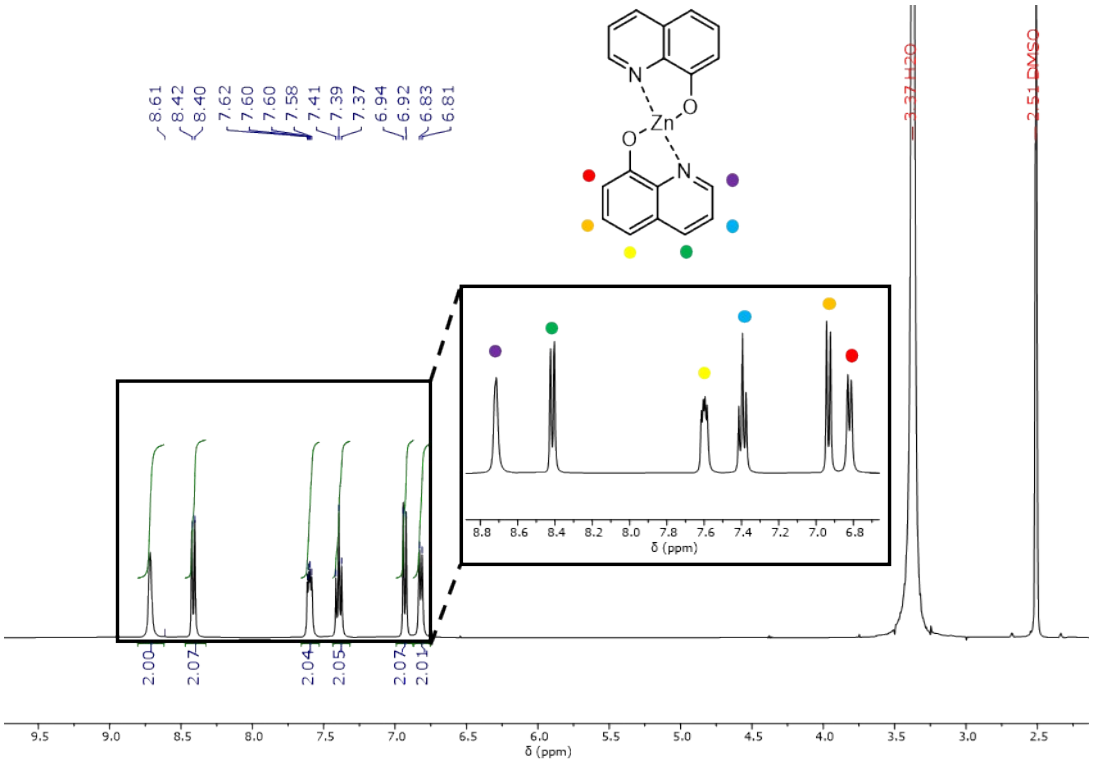

Figure S10. 1H NMR of crystals of **Zn(8-OH-quinolinate)$_2$** in DMSO-d$_6$ at 400 MHz, 25°C. The data are consistent with those reported in literature (see ref. 30-33 of the main text).

FT-IR

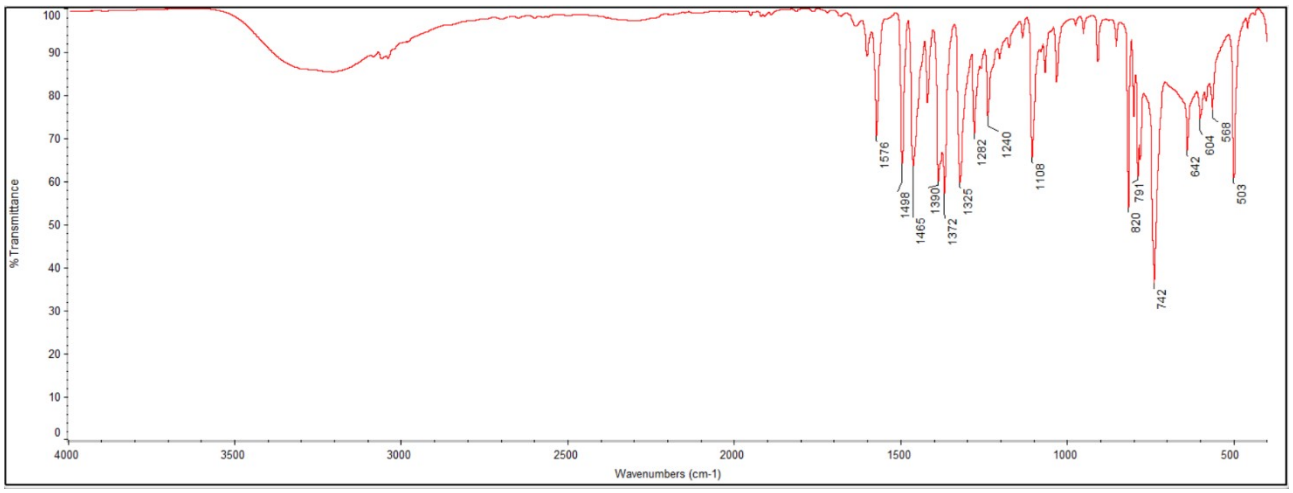

Figure S11. FT-IR (ATR) spectrum of the complex **Zn(8-OH-quinolinate)$_2$**. The spectrum is in accordance with literature reported data (see ref. 30-33). However, the large band above 3000 cm^{-1} might indicate the presence of water, as further corroborated by TGA analysis (see Figure S18).

Thermogravimetric Analysis

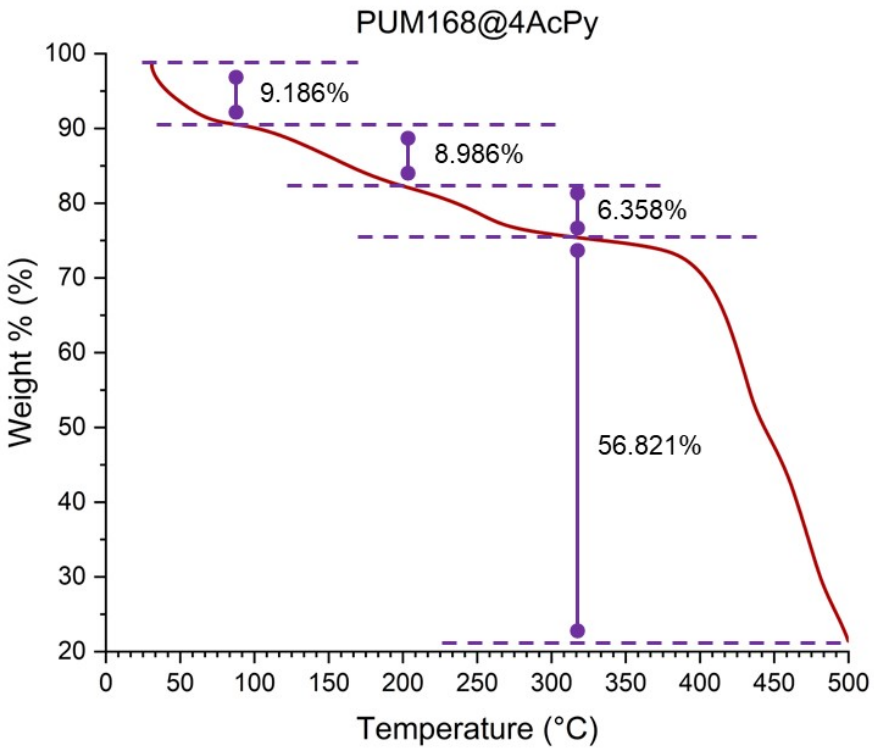

Figure S12. TGA trace for **PUM168@(4AcPy)** (air, 30-500°C, 10°C/min)

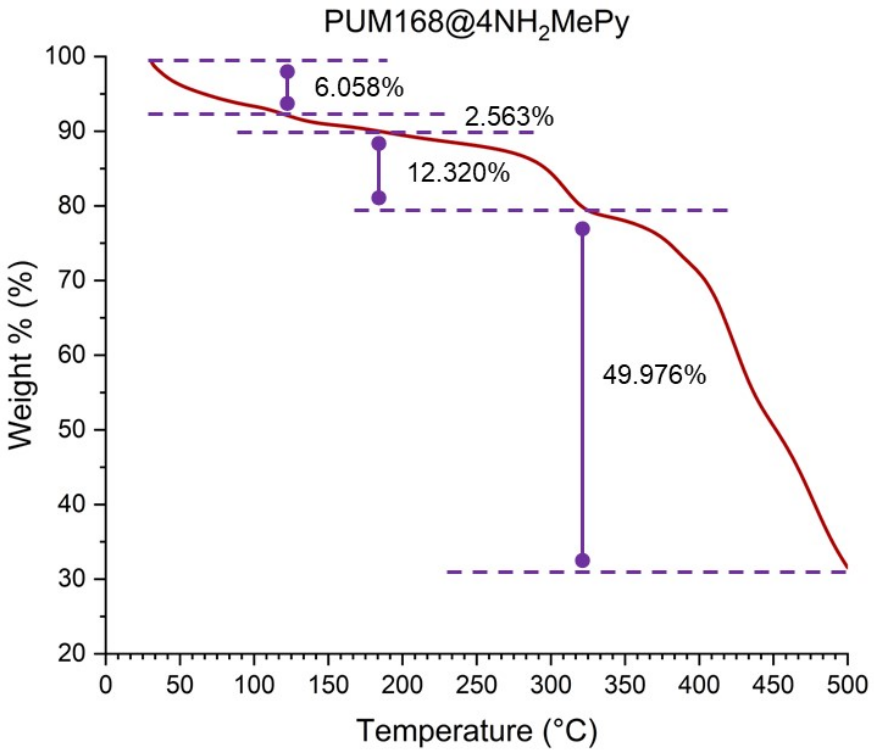

Figure S13. TGA trace for **PUM168@(4NH$_2$MePy)** (air, 30-500°C, 10°C/min)

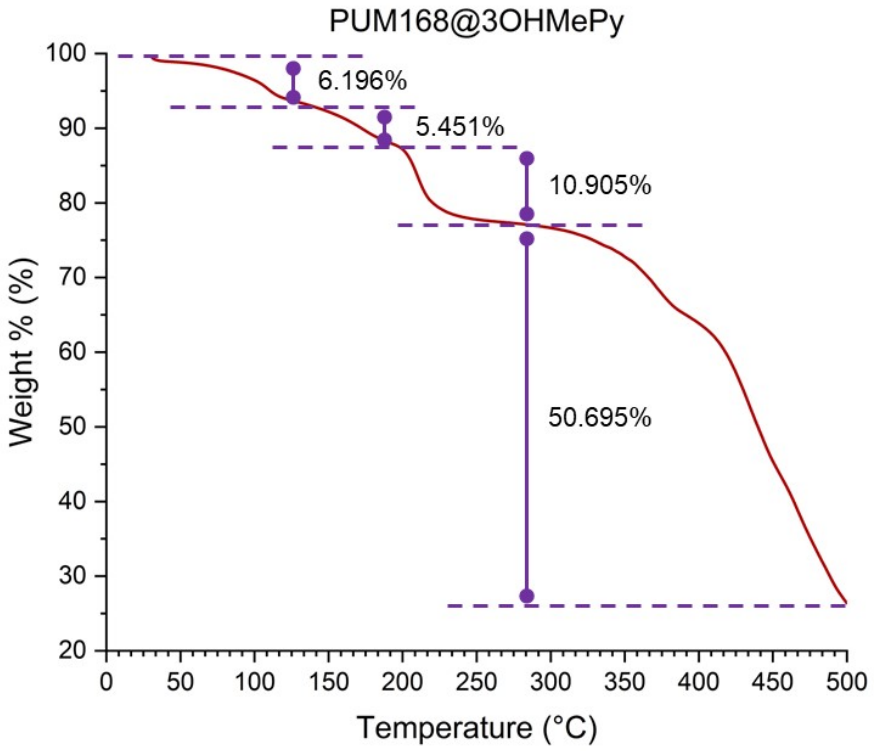

Figure S14. TGA trace for **PUM168@(3OHMePy)** (air, 30-500°C, 10°C/min)

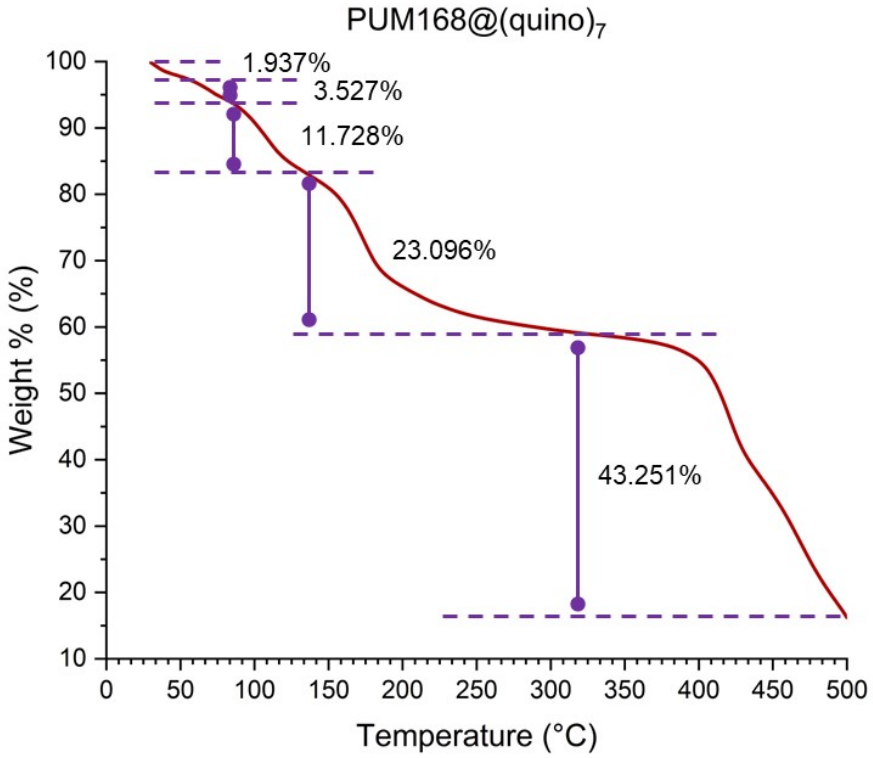

Figure S15. TGA trace for **PUM168@(quino)$_7$** (air, 30-500°C, 10°C/min)

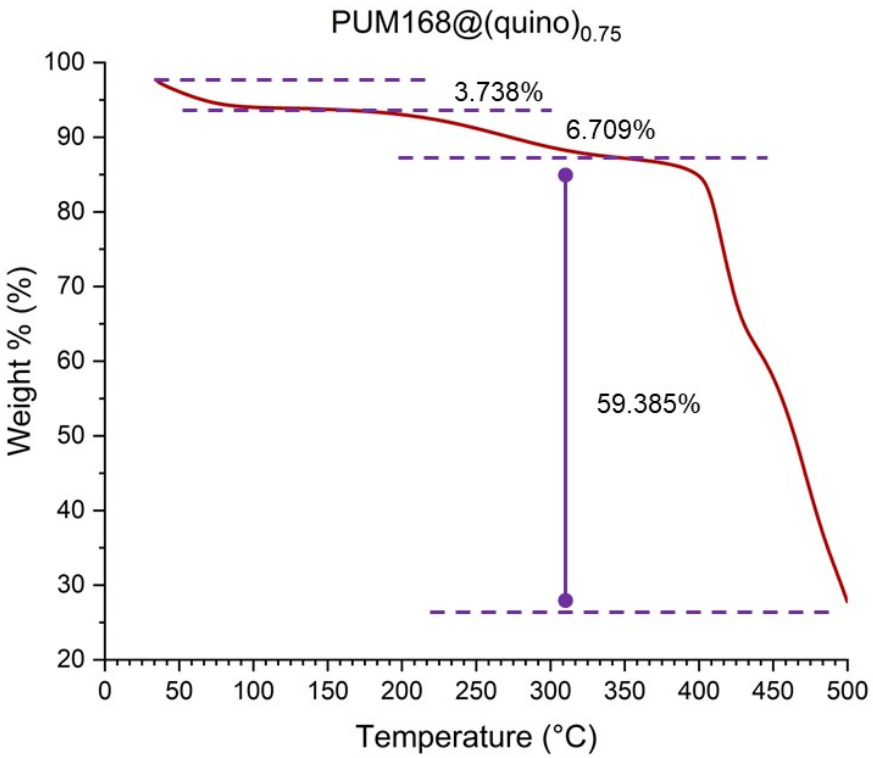

Figure S16. TGA trace for **PUM168@(quino)$_1$** (air, 30-500°C, 10°C/min)

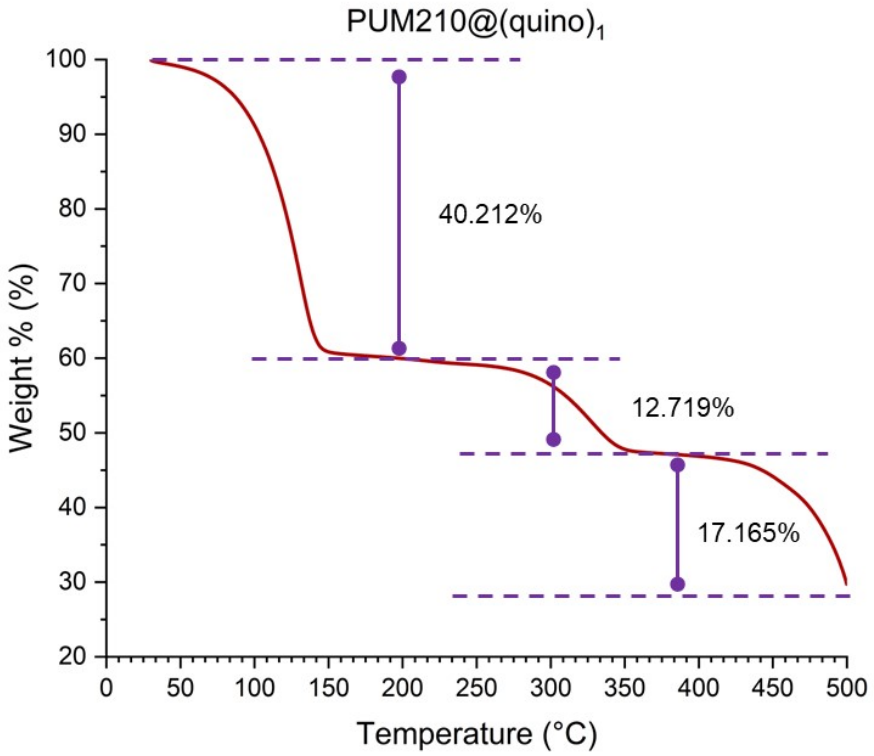

Figure S17. TGA trace for **PUM210@(quino)$_1$** (air, 30-500°C, 10°C/min)

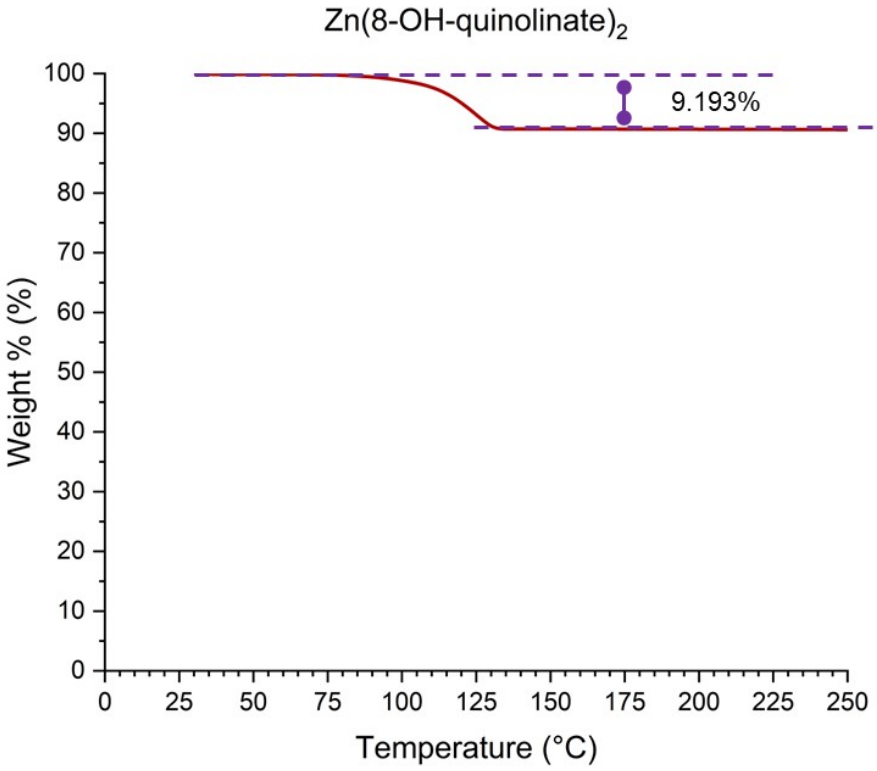

Figure S18. TGA trace for **Zn(8-OHquinolinate)$_2$** (air, 30-500°C, 10°C/min). The TGA trace presents a weight percentage loss of about 9.2% compatible with the removal of two molecules of water per Zn.

Scannning Electron Microscopy (SEM)

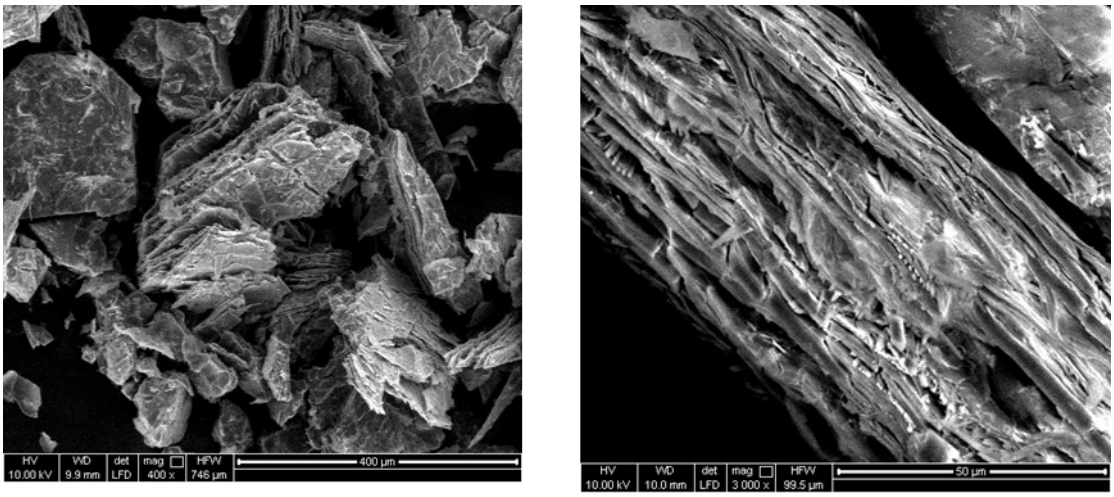

Figure S19. SEM images of **PUM168@Py** after 5 days of soaking. Left: 400X magnification to visualize the exfoliation of PUM168. Right: details on the exfoliation (3000X).

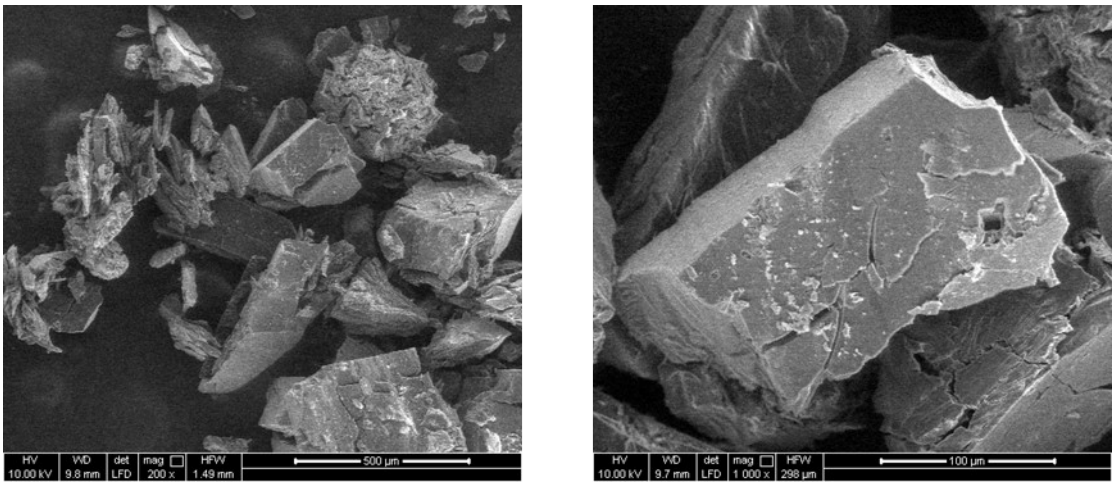

Figure S20. SEM images of **PUM168@(quino)$_7$** after 5 days of soaking. Left: 200X magnification to visualize the partial fragmentation of the crystals of **PUM168**. b) details on the cracks forming on the surface of block crystals of **PUM168**.

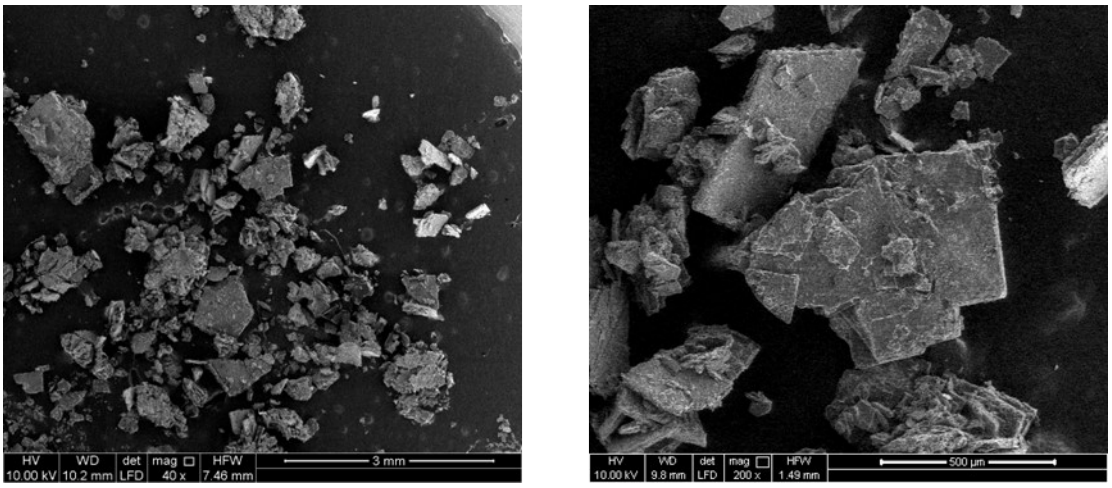

Figure S21. SEM images of **PUM210@(quino)$_1$** after 5 days of soaking. Left: 40X magnification to visualize the reduction in dimension of the crystals. Right: 200X magnification highlighting the preservation of the crystal quality.

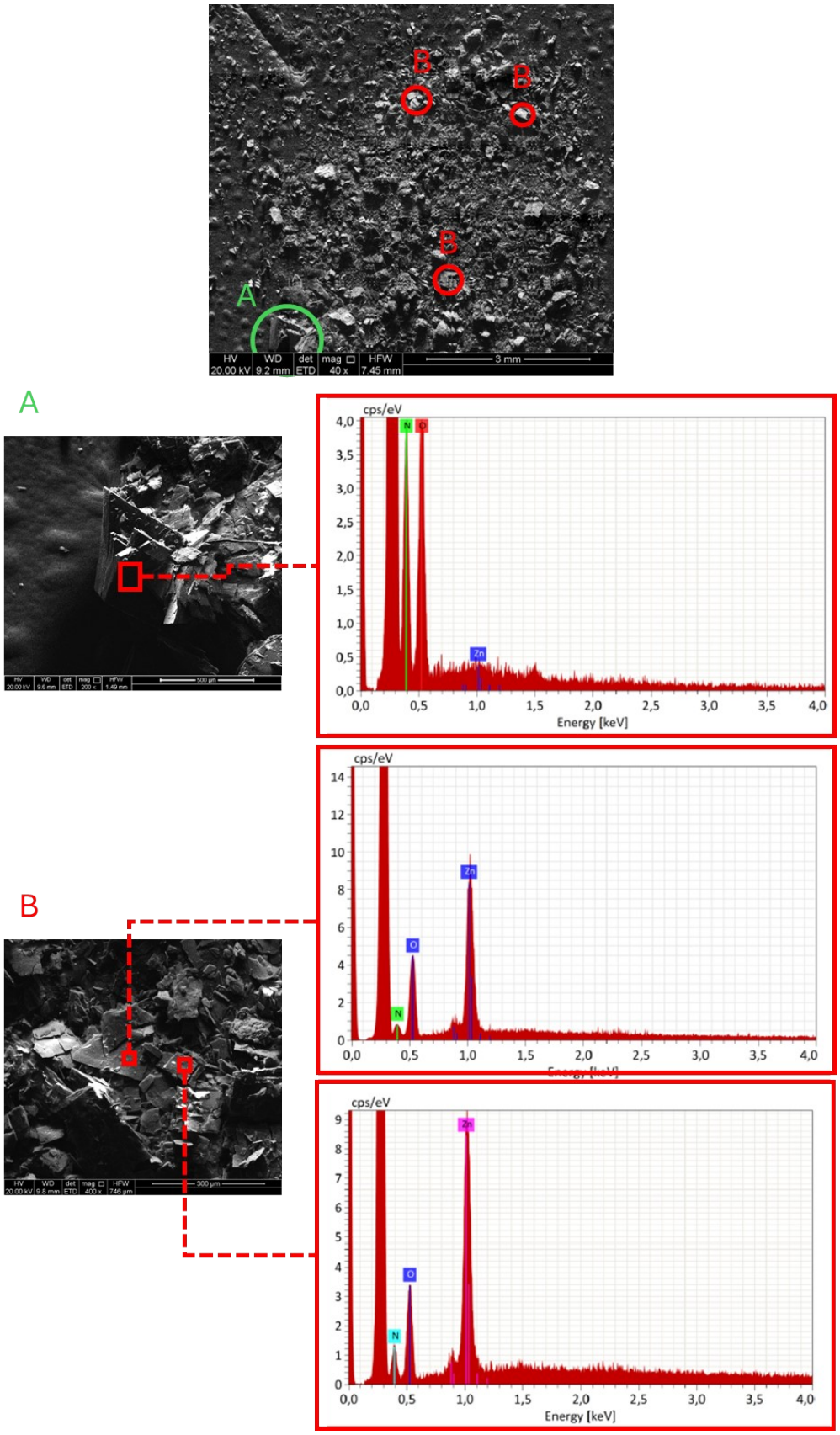

Figure S22. SEM images of crystals deriving from the soaking of **PUM210@DMF** in pyridine. The EDX analysis indicates that crystals labelled with A contain N and O but not Zn and are attributed to **L1**. The crystals labelled with B contain N, O and Zn and are attributed to **PUM210_PY**.

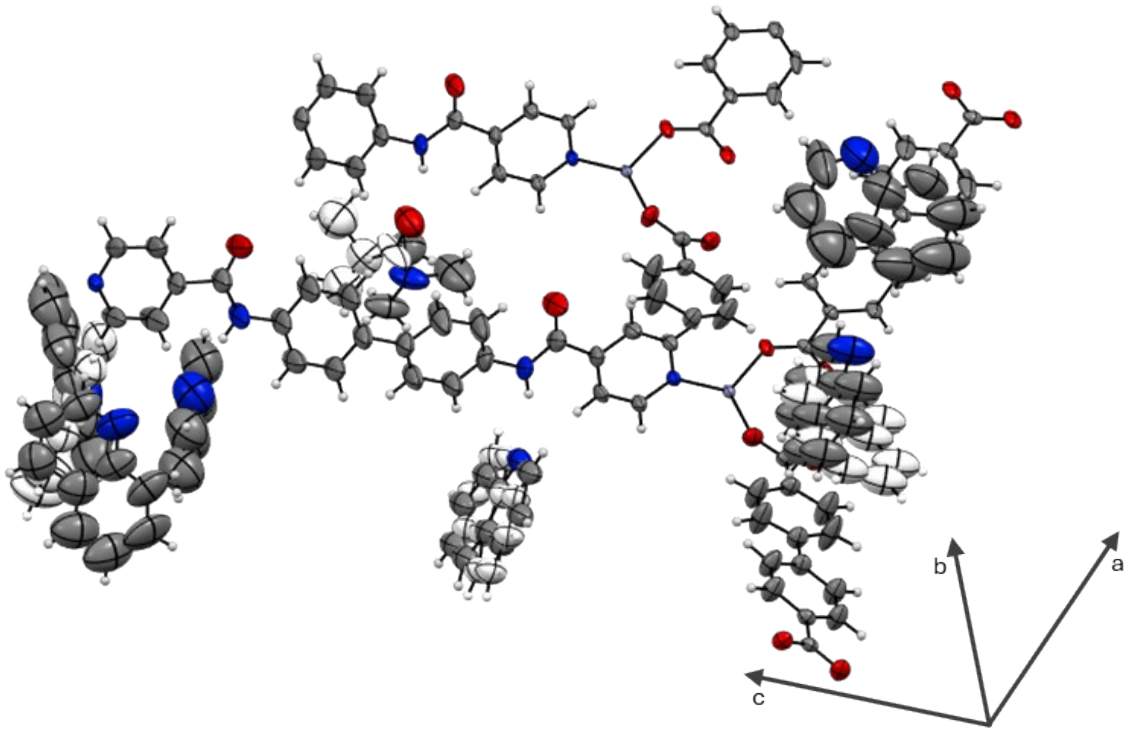

Figure S23. ORTEP visualization of the asymmetric unit of **PUM168@(quino)$_7$**. Disordered quinoline and DMF molecules are represented by element color and white, respectively. Thermal displacement ellipsoids are reported at a 50% probability level.

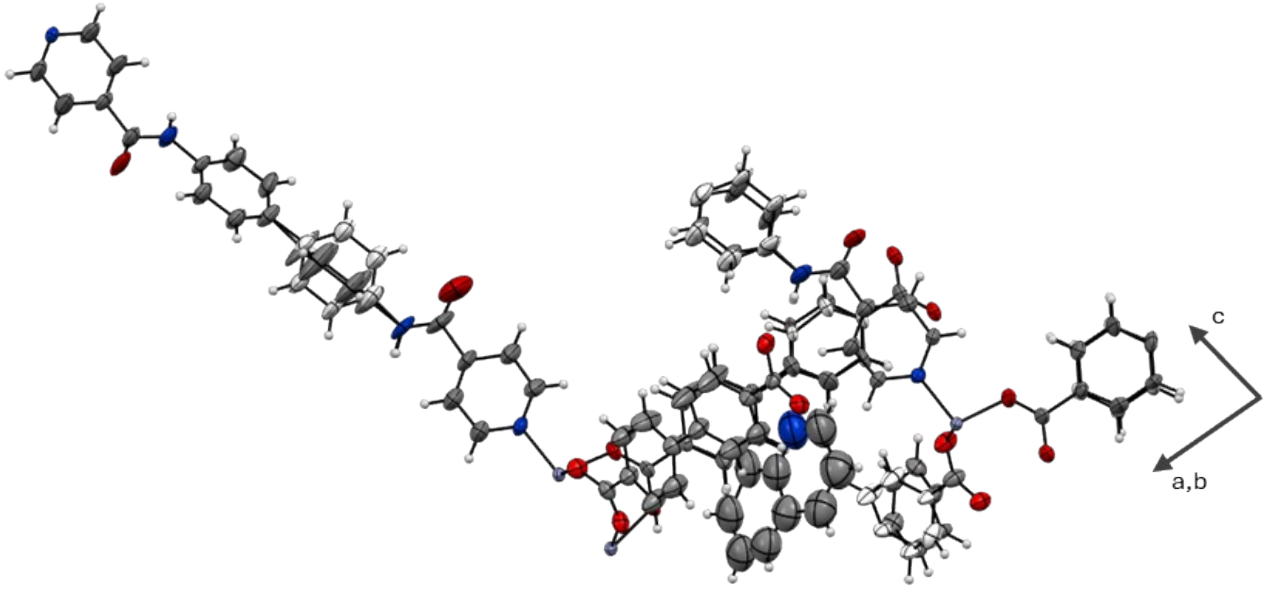

Figure S24. ORTEP visualization of the asymmetric unit of **PUM168@(quino)$_1$**. Disorder over the ligands is reported in white. Thermal displacement ellipsoids are reported at a 50% probability level.

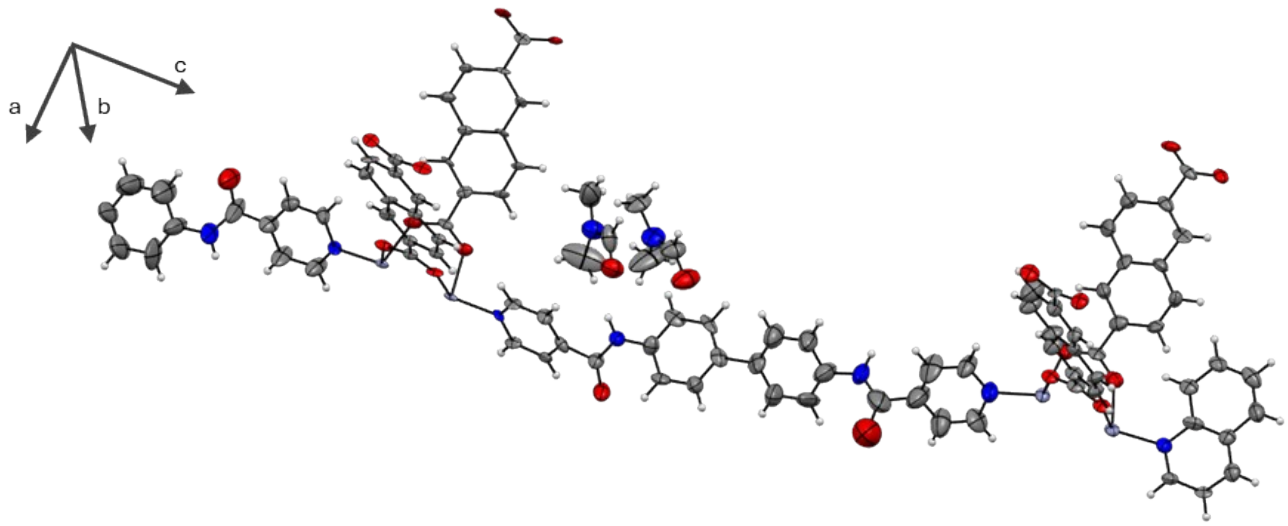

Figure S25. ORTEP visualization of the asymmetric unit of **PUM210@(quino)$_1$**. Disorder over the ligands is reported in white. Thermal displacement ellipsoids are reported at a 50% probability level. The

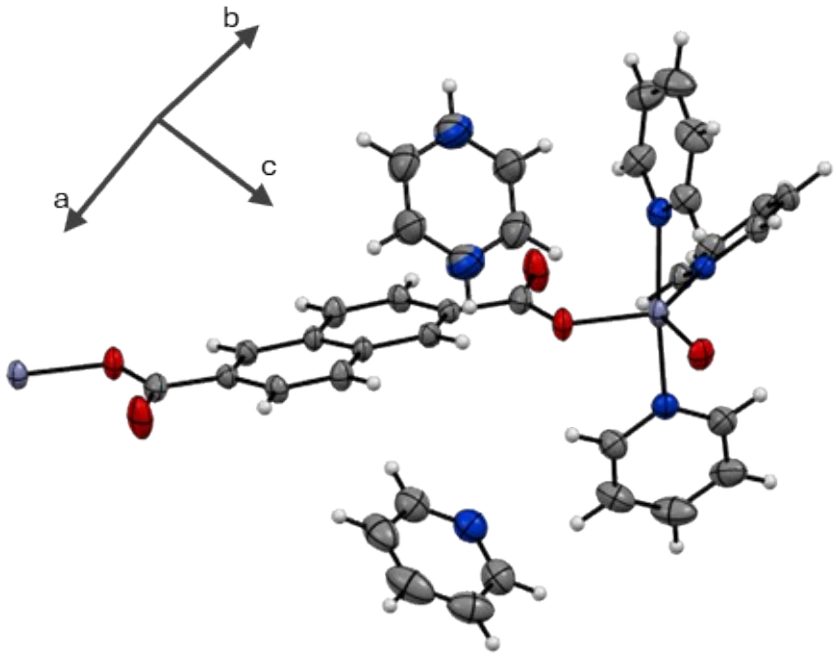

Figure S26. ORTEP visualization of the repetitive unit of **PUM210_PY**. Thermal ellipsoids are reported at a 50% probability level. The disorder over one of the included molecules of pyridine is reported.

Additional Structural Images

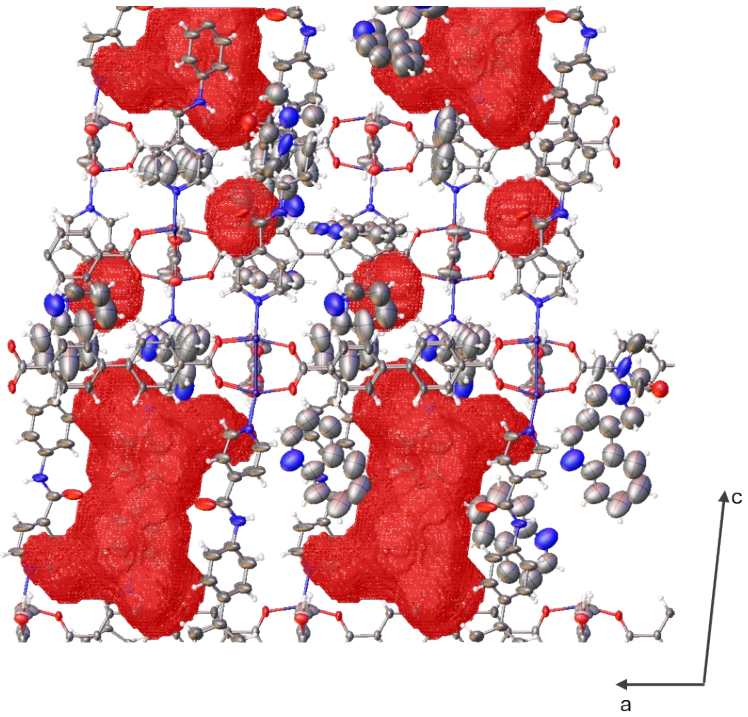

Figure S27. Visualization of the voids occupied by the residual electron density in **PUM168@(quino)$_7$**, represented by red wires and calculated by Olex2. The image is obtained from the GUI of Olex2.

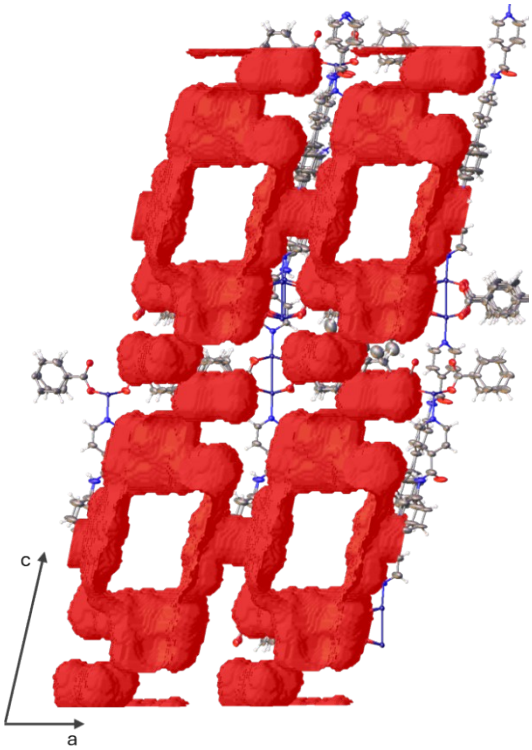

Figure S28. Visualization of the voids occupied by the residual electron density in **PUM168@(quino)$_1$**, represented by red wires and calculated by Olex2. The image is obtained from the GUI of Olex2.

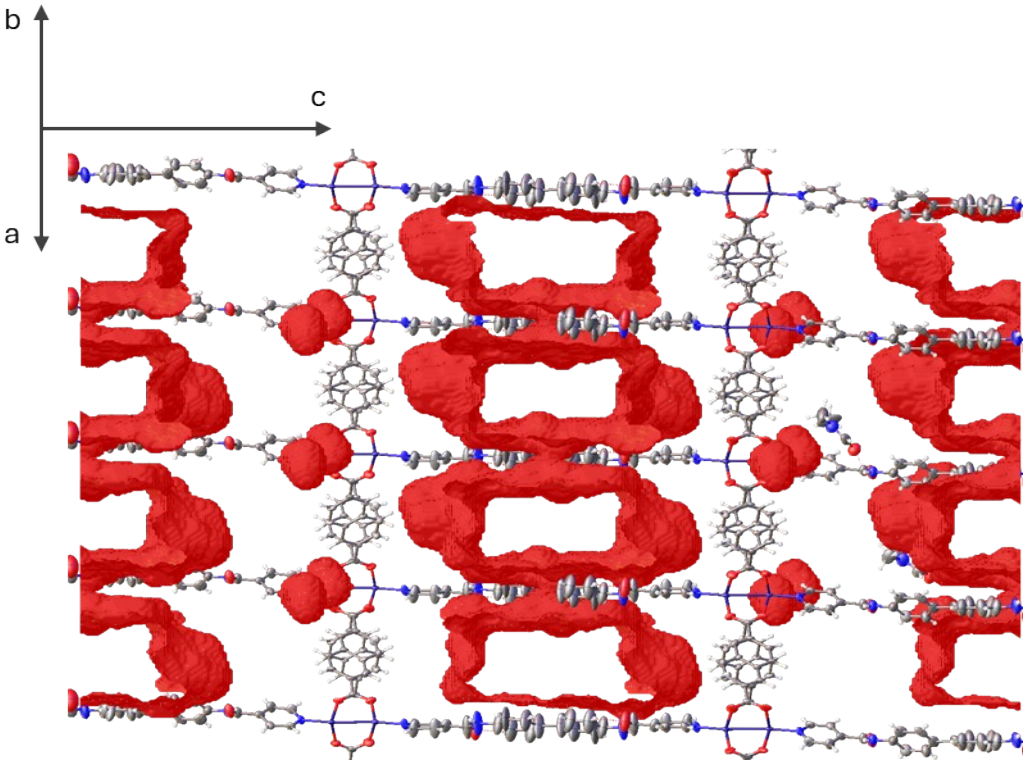

Figure S29. Visualization of the voids occupied by the residual electron density in **PUM210@(quino)$_1$**, represented by red wires. It is visible the presence of the elongated mono dimensional channels running along the crystallographic axis a. Moreover, the small pocket between the dicarboxylate layers is visualized. Only two out of the four catenations are represented for the sake of clarity. The image is obtained from the Olex2 GUI.

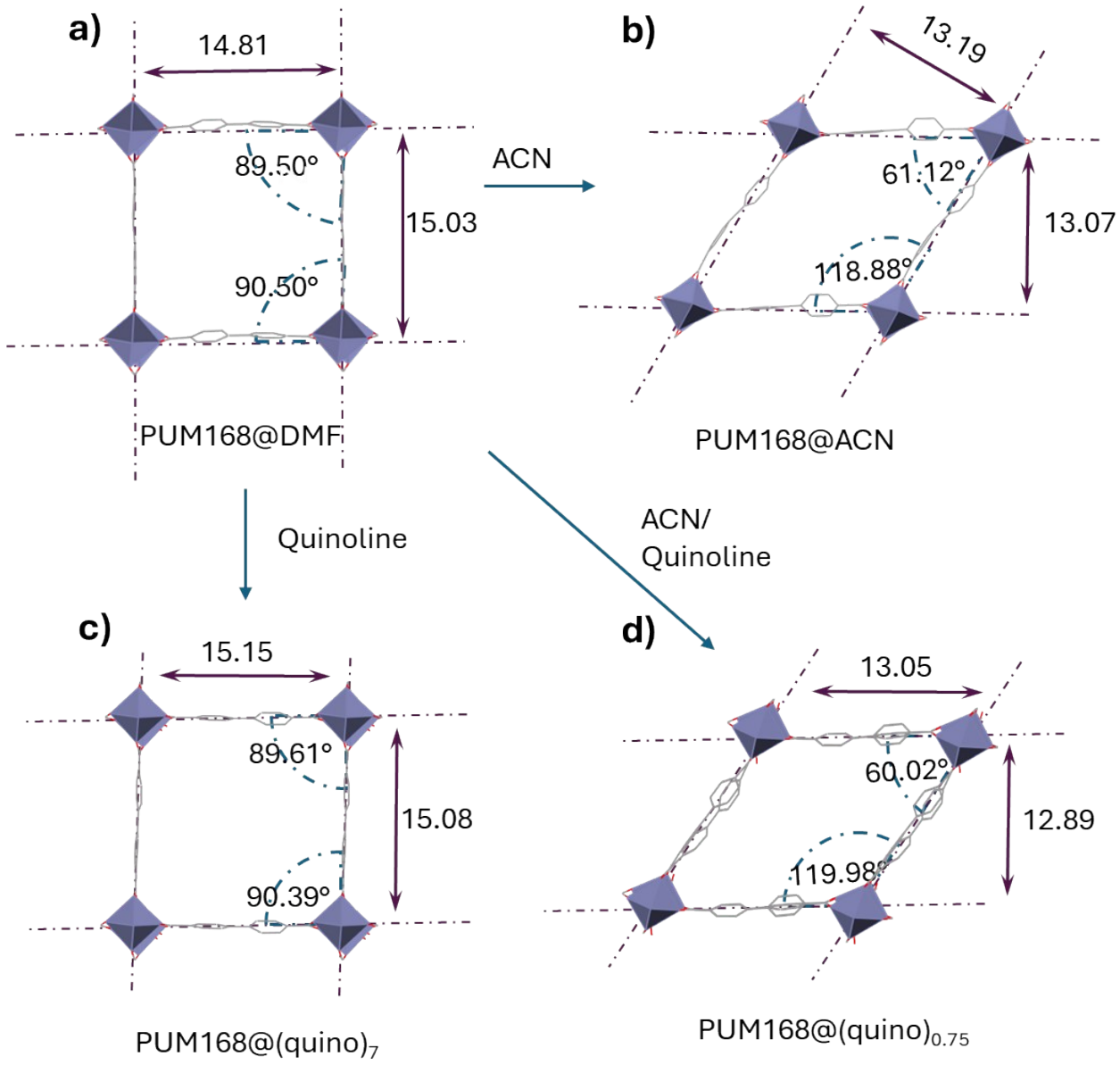

Figure S30. visualization of the distortion of one frame of PUM168 in four different situations: **a) PUM168@DMF**, showing the pristine squared grid displayed by the dicarboxylate layer; **b)** effect of acetonitrile over the angle on the dicarboxylate grid in **PUM168@ACN**; **c)** effect of the inclusion of neat quinoline, showing the retainment of the square grid in the structure of **PUM168@(quino)$_7$** and **d)** effect of the 0.1M ACN solution of quinoline. The structure of **PUM168@(quino)$_1$** shows angles comparable with the one determined for **PUM168@ACN**.

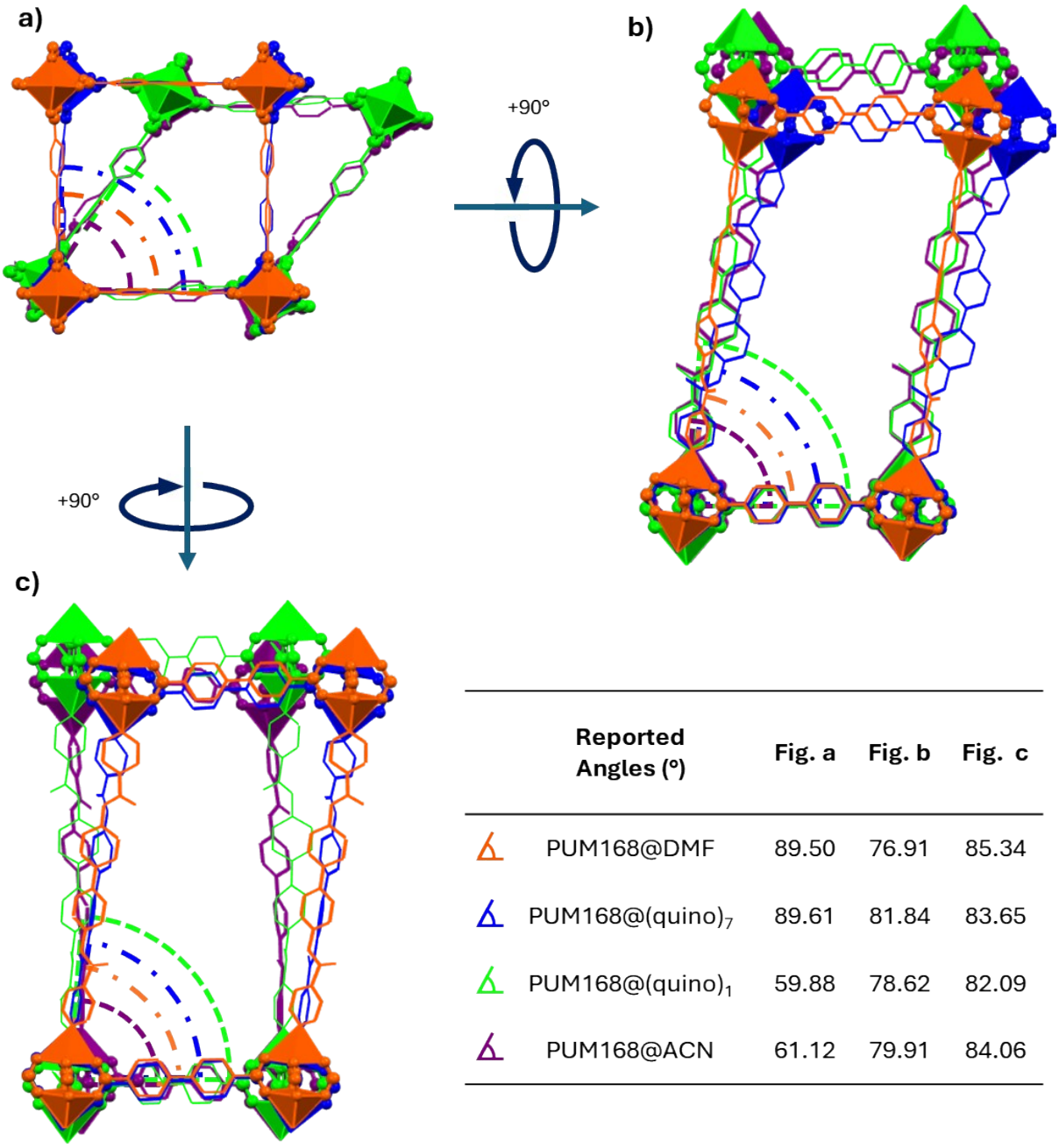

	Reported Angles (°)	Fig. a	Fig. b	Fig. c
∠	PUM168@DMF	89.50	76.91	85.34
∠	PUM168@(quino)$_7$	89.61	81.84	83.65
∠	PUM168@(quino)$_1$	59.88	78.62	82.09
∠	PUM168@ACN	61.12	79.91	84.06

Figure S31. Comparison between the angles featuring the framework in **PUM168@DMF**, **PUM168@ACN**, **PUM168@(quino)$_7$** and **PUM168@(quino)$_1$**. The similarities between the structure of **PUM168@DMF** and **PUM168@(quino)$_7$** and between **PUM168@ACN** and **PUM168@(quino)$_1$** are highlighted by the calculated angles reported in the table.

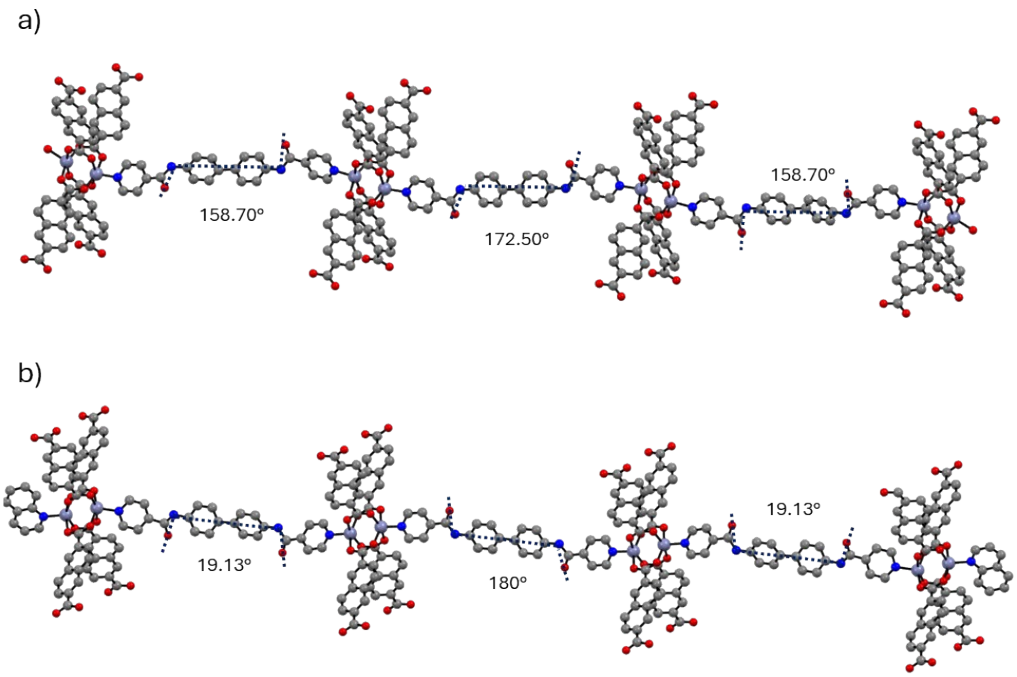

Figure S32. Comparison between the torsional angles of the ligands **L1** in a) **PUM210@DMF** and b) **PUM210@(quino)$_1$**. In the structure of **PUM210@(quino)$_1$** the two distal ligands L1 are adopting a cisoidal conformation, changing from the starting staggered disposition.

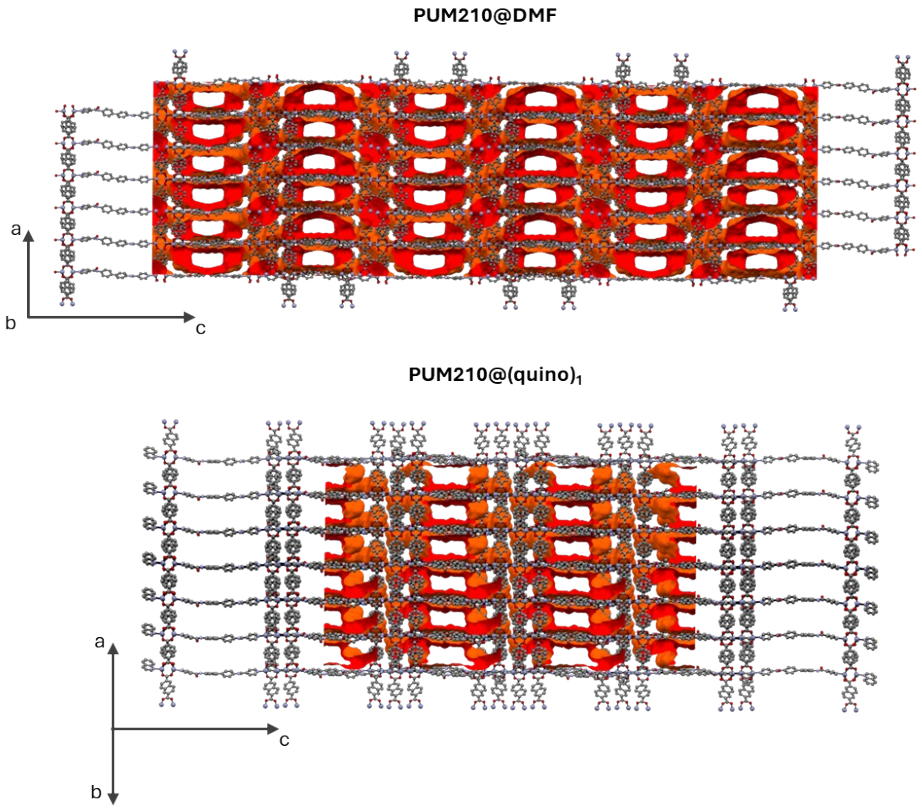

Figure S33. Comparison between the disposition of the mono dimensional channels running along the crystallographic ***b*** axis in **PUM210@DMF** (top) and along the diagonal of the crystallographic plane passing through ***a,b*** in **PUM210@(quino)$_1$** (bottom).

Powder X-Ray diffraction (PXRD)

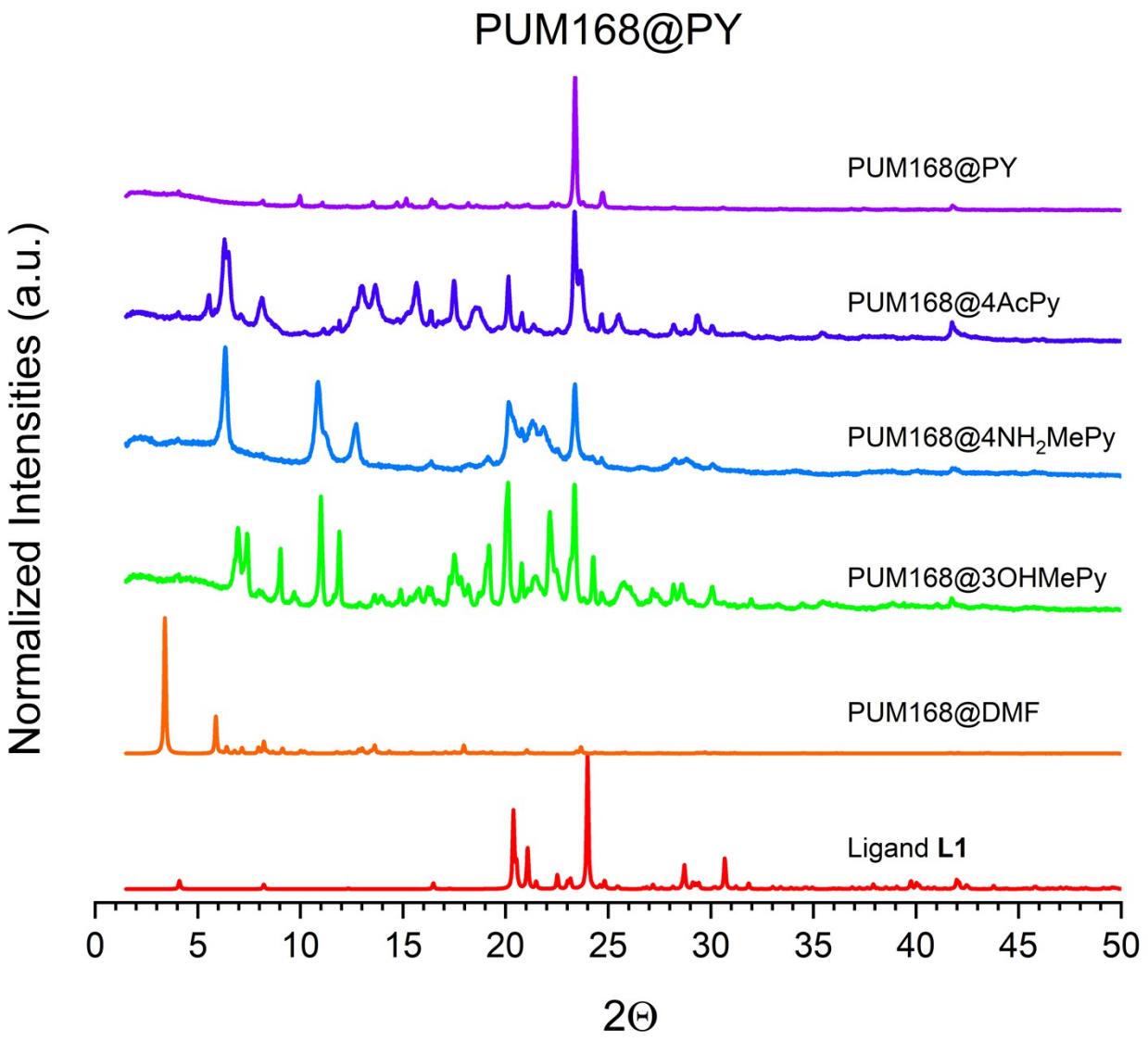

Figure S34. Comparison between the powder X-ray diffractogram of PUM168 after treatment with different pyridines. The formation of different phases can be seen by comparison with the calculated PXRD of the ligand **L1** (reference: structure PASLUT) and the calculated PXRD for PUM168@DMF (refence: TOTMOH).